Journal of Physics: Conference Series

PAPER • OPEN ACCESS

Towards the development of smart weather routing systems for leisure planing boats

To cite this article: M Ciampolini *et al* 2022 *J. Phys.: Conf. Ser.* **2385** 012068

View the article online for updates and enhancements.

You may also like

- Infrared Photometric Study of Wolf–Rayet Galaxies
P. S. Chen, X. H. Yang, J. Y. Liu et al.
- Hull Surface Information Retrieval and Optimization of High Speed Planing Craft
A F Ayob, W B Wan Nik, T Ray et al.
- Wolf–Rayet Galaxies in SDSS-IV MaNGA. I. Catalog Construction and Sample Properties
Fu-Heng Liang, , Cheng Li et al.

This content was downloaded from IP address 150.217.19.161 on 17/04/2023 at 13:41

Towards the development of smart weather routing systems for leisure planing boats

M Ciampolini, F Balduzzi, L Romani, L Bellucci, A Bianchini and G Ferrara*

Department of Industrial Engineering, Università degli Studi di Firenze, via di Santa Marta 3, 50139 Firenze, Italy

*Contact author: giovanni.ferrara@unifi.it

Abstract. Weather routing (WR) systems are widely adopted in the maritime transport since safety of goods and saving of fuel are crucial for shipping companies. However, the need of protecting the local coasts and reducing CO_2 emission is making WR attractive even for the market of leisure boats, especially if comfort and safety are also accounted. In the present study, a prototype of a WR system is presented. The developed tool implements the Dijkstra's algorithm to find the fuel-optimal path while ensuring comfort and safety. A computationally efficient digital twin of a planing boat, based on a 2D+t model and a powertrain mapped model, has been implemented for the estimation of the fuel consumption and the evaluation of vertical accelerations. The methodology for the acquisition of online weather data is presented, together with the strategy for the assessment of comfort and habitability. The application of the WR tool in a typical path of the Tuscan Archipelago shows improvements in fuel usage and comfort even in moderate weather conditions. The influence of each weather variable on fuel efficiency is assessed, highlighting the requirement of an accurate dynamic modelling. Criteria for the graph design are also outlined, showing a wrong estimation of comfort and fuel usage in case of low-definition graphs. The paper proves the potential and the effectiveness of the developed tool, moving toward a greener and more comfortable navigation in local seas.

1. Introduction

New requirements are about to be introduced by local authorities to reduce pollution of local waters and CO_2 emission. The 2018 Initial IMO (International Maritime Organization) GHG Strategy moves toward the reduction of at least 50% of the annual greenhouse gas emission from international shipping by 2050 compared to 2008, thus requiring further improvements in the powertrain efficiency. The IMO does not deal with leisure crafts so far, but the recent application of the IMO TIER III limits to 24-meter boats indicates how the legislation is moving toward greener limits even for smaller boats.

In this perspective, the application of methane and diesel-electric powertrains, usually investigated in transport and cruise ships, seems unfeasible in recreational crafts due to encumbrances, system complexity, and weight. Thus, interest in hybrid powertrains has been growing recently, although it still represents an unconsolidated market. While waiting for greener propulsion technologies, weather routing (WR) navigation systems could be adopted in planing leisure crafts to reduce CO_2 emissions and to ensure comfort and safety of onboard passengers. However, despite WR is widely adopted in the transport sector for the safety of goods and fuel savings, it is not diffused in the boating sector.

According to Wang et al. [1], different algorithms can be adopted in WR. Lee et al. [2] classified these algorithms in cell-based, i.e., unsmooth path (Dijkstra algorithm and A-star algorithm), and cell-

Content from this work may be used under the terms of the Creative Commons Attribution 3.0 licence. Any further distribution of this work must maintain attribution to the author(s) and the title of the work, journal citation and DOI.
Published under licence by IOP Publishing Ltd

free. i.e., smooth path, (isochrone method, dynamic programming, and genetic algorithm). Walther et al. [3] instead noted that the selection of the appropriate algorithm depends on the desired objectives, control variables, and constraints, as well as implementation (e.g., hardware).

Regarding cell-free methods, the historical approach is the isochrone method (IM) for navigation time reduction, which software implementation was proposed by Hagiwara and Spaans [4]. As stated by Rabaud [5], IM is nowadays commonly adopted in sailboats. Despite the relatively low calculation time, IM is not suited for accounting for constraints. In fact, e.g., Szlapczynska and Smierzchalski [6], required an evolutionary approach to include land zone constraints in an IM-based WR model.

The dynamic programming (DP) is another widespread approach, in which WR is considered an N-stage decision process (Zoppoli [7]). Time, distance, and fuel usage can all be used to define stages since they all monotonically increase during navigation; furthermore, differently than IM, constraints can be easily implemented. Aligne et al. [8] found the forward recursive application to be preferable, allowing real-time meteorological updates. Recently, the 3-D DP, involving two control variables, has been proposed. Aligne et al. [8] and Shao et al. [9], e.g., varied vessel heading and powertrain power to minimize respectively voyage time and fuel consumption, accounting for safety constraints (surf-riding and rolling motion) and land zones. Zaccone et al. [10] instead varied heading and speed to reduce fuel consumption, while accounting for safety (Lateral Force Estimator) and comfort (Motion Sickness Index). The DP is a time effective WR methodology, but it seems appropriate for ocean navigation only; in fact, it can be thought the rapid variation of weather conditions and the different obstacles along coastal paths may not make the Bellman's principle always applicable.

Genetic algorithm (GA) has gaining interest as a multi-objective optimization tool. The population comprises multiple individuals which are represented by a series of latitude and longitude coordinates; however, chromosome structure can also include engine settings, vessel velocity, or even uncertainty of data (Szlapczynska and Smierzchalski [6]). Kim and Kim [11], e.g., introduced a safety-based GA model to determine the route with minimum average towing tension while respecting time constraints. Hinnenthal and Clauss [12] instead accounted for the stochastic behaviour of weather to optimize time, fuel consumption, safety, and comfort. Lee et al. [2] finally used a non-dominated sorting GA for choosing path and speed profile so as to minimize fuel consumption, while accounting for time and engine operating range constraints, as well as earth zones. The major issue of GA lies in calculation time, tending to be well higher than that of deterministic or graph-based methods.

Concerning the cell-based methods instead, the most diffused approach is the Dijkstra's algorithm (DA), which is a graph-based minimum-cost path finding algorithm with a single objective function and implicitly defined constraints. Takashima et al. [13] showed a constant-propeller speed WR model for coastal merchant ships based on DA for fuel optimization. Sen and Pahdy [14] developed instead a DA-based time optimization WR model accounting for voluntary and involuntary speed reduction and land constraints. Mannarini et al. [15] adopted the DA to minimize travel time while respecting safety restrictions of IMO. Finally, Pennino et al. [16] proposed a DA-based WR model for seakeeping improvement in transoceanic routes. Major issues of the application of the DA in WR concerns the long calculation time (Walther [3] suggests its use in coastal shipping and short routes only), the low path smoothness, and the singular objective function. However, it explores a wide set of possible solutions, and the chosen path always represents the exact solution.

Although several efforts have been made to design increasingly effective and versatile WR models for use in navigation systems of cargo and transport ships, to the best of Authors' knowledge planing leisure crafts have not been considered to date. This can be probably attributed to the need of small computational times, which limits the dynamic modelling to correlative approaches and/or simplified longitudinal and vertical balance of forces. Dealing with planing crafts instead more detailed dynamic models should be used since computationally efficient models like Savitsky's [17] are not adequate for wavy seas. Moreover, hull dynamics in waves should be carefully assessed to evaluate habitability, especially considering that a regulation for the definition of comfort and safety in leisure boats is missing. This requirement can nowadays be matched thanks to the latest electronic technologies, which strongly improved the computational possibility of onboard computers.

In the present paper, a methodology for the development of a WR navigation system based on DA for use in leisure planing crafts is presented. The tool adopts a detailed 2D+t model previously developed by the same authors in [18] for the prediction of hull dynamics and forward resistance in waves. Comfort of passengers is assessed following the procedure of the ISO 2631 regulation and applied as a constraint. A methodology for the real-time acquisition of weather data from the LaMMA Meteo database is also presented. The application of the WR model on the Tuscan Archipelago will show the potential of reducing fuel usage, while ensuring comfort and safety. Different applicative examples will define the guidelines for the future development of an industrial prototype.

2. Materials and method

The proposed weather routing (WR) numerical tool was developed in the MATLAB® ambient. Data of waves are acquired in terms of significant wave height and significant wave period (as they are presented in the LaMMA website), and it is assumed that the Airy wave theory can be applied to calculate the wave celerity; sea currents are instead neglected. Wind is assumed to be steady-state and the mean value of each band of the Beaufort scale is considered. Finally, the effects of waves and wind on the boat are considered to affect the boat longitudinal dynamics only, independently from the direction (e.g., wind acting normal to the forward speed equals to null wind); thus, roll motion is not considered.

The WR code is made of three main modules:

- a computationally efficient MATLAB® Simulink® digital twin of the test case boat, aimed at the prediction of fuel consumption, safety, and comfort, in front of some weather input data,
- a sub-code for the acquisition of geographical and weather data from the "LaMMA Mare e Vento" website, which discretizes the geographical map into rectangular cells and assigns to each cell the weather conditions (intensity and direction of wind and waves), and
- a master-code for the application of the Dijkstra's algorithm, which: i) draws the direct graph on the map and assigns to each node the weather conditions, ii) launches the digital twin to evaluate the weights of each graph connection, and iii) runs the DA highlighting the optimal path and the unsafe sub-routes.

The interaction between the modules of the WR model is presented in figure 1.

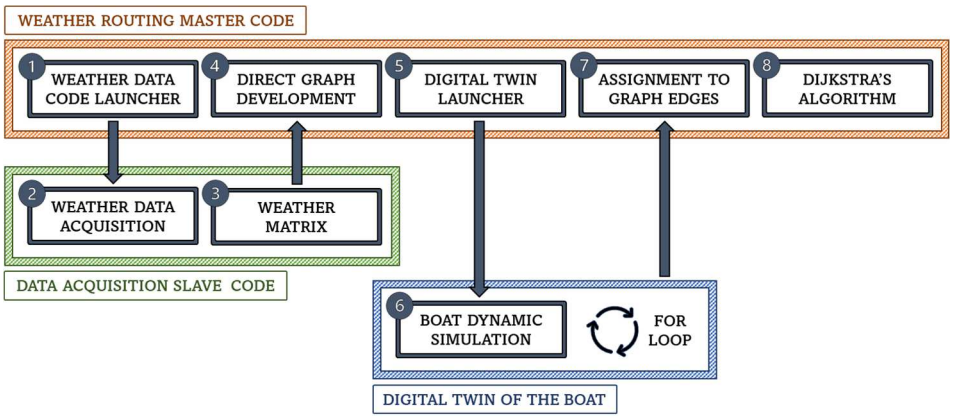

Figure 1. Interactions between the various modules of the developed WR code.

The dynamic modelling of the digital twin, as well as the criterion for accounting for passenger comfort, have already been presented in [18]; thus, only the mean features concerning the interaction between the vessel and the weather conditions (wind and waves), and the powertrain modelling are resumed in the present paper for the sake of completeness.

2.1. Test case

A medium/small leisure fishing boat was chosen as the test case for the digital twin, representing an example of a coastal recreational craft, i.e., the YANMAR EX34 fishing cruiser. The boat topside is of flybridge type. The hull is of warped planing type, tending to be flat by moving toward the stern. The main features of the test case are presented in table 1.

Table 1. Characteristics of the YANMAR EX34 planing boat.

Length LOA [m]	Width [m]	Depth [m]	Raw weight [kg]	Engine type	Power (max)	Propeller type
10.63	3.30	1.90	4990	6LY440J	324 kW	3-620x885

Inertial characteristics were estimated by means of a dedicated CAD model by positioning different concentrated masses (powertrain, fuel tank, and passengers). The predicted weight under load was found to be 6104 kg and the projected chine length at rest 8.56 m.

2.2. Digital twin

As known, a digital twin is a virtual replica of a real-world system capable of digitally mirroring its behavior in front of any external (e.g., boundary conditions) or internal scenarios (e.g., a different component), allowing a reduction of manufacturing costs and the development of innovative model-based devices (e.g., smart navigation systems). In case of planing crafts, it must be able to reliably represent the dynamics, the energy fluxes, and the comfort of onboard passengers.

Focusing on the programming ambient, MATLAB® Simulink® was chosen since it allows the design of off-line models, which can be used, e.g., for energy analyses, but also the implementation of real-time models in model-in-the-loop applications, as required in navigation systems.

Figure 2 presents the data flow of the proposed digital twin. In addition to the characteristic curves of the powertrain components and the propeller, the inputs of the twin concern few geometrical parameters, such as the projected hull length, the behavior of the beam at the chine (or the deadrise), the position of the center of gravity (CG), the inertial terms, the characteristics of the appendages, the position of the average center of pressure (CoP) of the topside, the target speed, and the numerical setup. In this way it is thus possible to represent any recreational planing boat by varying the inputs in the initialization function.

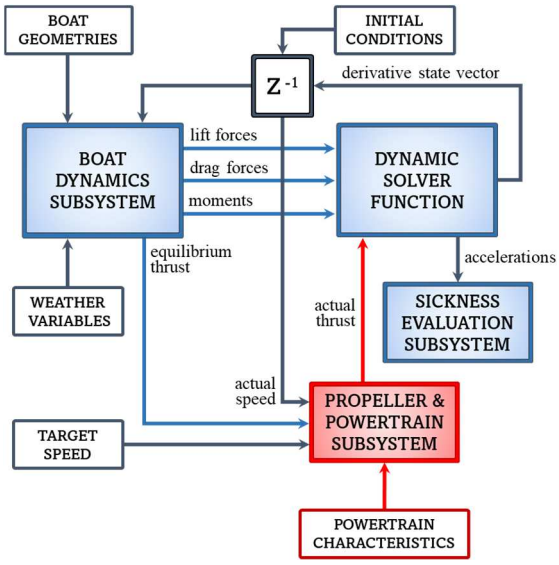

Figure 2. Operating principle of the digital twin of the YANMAR EX34 planing boat. Blue background boxes concern the simulation of boat dynamics; the red block concerns the simulation of the powertrain.

The proposed digital twin is composed of four main parts:

- the "Boat Dynamics" subsystem, implementing the 3-DOF 2D+t dynamic model, providing all the forces acting on the boat, in addition to the indication of the propeller position (with respect to the sea level) and the thrust required to the equilibrium on the horizontal axis,
- the "Propeller and Powertrain" subsystem, implementing a mapped model of the powertrain, which provides the actual thrust of the propeller passing through the powertrain components and the control logics, in addition to the torque correction signal required to correct the possible gaps between the desired and the actual speeds,
- the "Dynamic Solver" function, implementing the Runge-Kutta numerical method, in which the three equations of motion are solved to update the state variables, and
- the "Sickness Evaluation" subsystem, implementing the filters of the ISO 2631 regulation, which provides the Vibration Dose Value (VDV) and Root Mean Square (RMS) acceleration at the passenger seats, simulating the healthiness of onboard passengers.

2.2.1. Boat dynamics modelling. The 3-DOF (surge, heave, pitch) 2D+t model acting as dynamic core of the computationally efficient digital twin has been already presented in detail and validated in a previous work [18]. In the present section only the main features concerning the modelling of the interaction between the boat dynamics and wave/wind conditions are thus resumed.

In general terms, the hydrodynamic modelling follows the 2D+t methodology of Zarnick [19]; thus, as in the strip theory, forces are evaluated strip-by-strip and then integrated along the entire hull length. The hydrodynamic force, f_h, acting on a generic section of the hull (normal to the keel line) is supposed to be equal to the change of the fluid momentum:

$$f_h = -\frac{D}{Dt}(m_a V) \tag{1}$$

where m_a is the sectional added mass and V is the relative velocity (normal to boat axis) between the keel line of the section and the sea. It is worth noting that V accounts for the wave vertical orbital velocity, thus implicitly including the wave elevation. The crossflow drag term, typically adopted in 2D+t models in order to account for the increase of the added mass in wet-chine conditions, is not included since the incremental added mass coefficient of Payne [20] is considered. This assumption leads to the following formulation of the sectional added mass:

$$m_a = C_{m0}\left(1 + k_m \frac{z_c}{B_m}\right)\rho\frac{\pi}{2}b^2 \tag{2}$$

where z_c is the chine immersion, B_m is the beam of the section, C_{m0} is the deadrise-dependent added mass coefficient of Wagner [21] and k_m is the deadrise-dependent corrective term proposed by Payne [22]. The wetted half-beam (b) depends on the chine sinkage, and it corresponds to the half-beam in wet-chine conditions and to:

$$b = \frac{d_e}{tan\beta} \tag{3}$$

in dry-chine conditions. The wetted half-beam thus accounts for the effective depth of penetration of the section (d_e), in which the water pile-up is included by means of the pile-up coefficient (C_{pu}):

$$d_e = C_{pu}d = C_{pu}\frac{z_k - r}{cos\,\theta} \tag{4}$$

where r is the wave elevation, θ is the pitch angle and z_k is the vertical position of the keel line. The formulation of Payne [20] is adopted for the pile-up coefficient. It is worth pointing out that, dealing with a 3-DOF model, the wave direction (with respect to the boat horizontal axis), μ, is accounted in the wave elevation:

$$r = r_0\,cos(kxcos\mu - \omega t) \tag{5}$$

where r_0 is the wave amplitude, k the wave number, ω the wave frequency, and t the time.

As stated by Zarnick [19], the forces due to waves are implicitly accounted by assuming that the wave excitation is caused by the alteration of the wetted length and the draft of the hull and by the vertical component of the wave orbital velocity at the surface altering the normal velocity. However, diffraction forces are missing. Thus, in order to account for the effects of diffraction forces on the sole surge equation, the Faltinsen's asymptotic formula [23] was considered:

$$R_{aw} = \frac{\rho g r_0^2}{2} \int_C \left\{ sin^2(\theta_w + \alpha_w) + \frac{2\omega \dot{x}}{g} [1 - cos\,\theta_w\, cos(\theta_w + \alpha_w)] \right\} sin\,\theta_w\, dl \qquad (6)$$

where θ_w is the curvature of the hull and α_w is the wave propagation direction with respect to the x-axis (0° for heading waves). Since it applies only to blunt ships, a corrective term based on wave height (H), and wavelength coefficient (c_λ) was introduced to make it suited for planing hulls:

$$R'_{aw} = R_{aw} \left(-6.731 \frac{H}{B} + 2.718 \right) \left(0.5 + \frac{1}{0.798\sqrt{2\pi}} e^{-\frac{(c_\lambda - 0.125)^2}{0.0072}} \right) \qquad (7)$$

The effects of following and quartering waves on the resistance are usually assumed to be small; thus, they have been excluded in the computation of the added resistance.

It should be pointed out that the developed 2D+t model accounts for the contribution of buoyancy, skin friction, whisker spray, and appendages on lift and drag forces; an accurate description of the modelling technique is presented in [18].

Concerning the interaction between the boat topside and wind flow, only the projection of the wind speed along the horizontal axis ($\dot{x}_w$), assumed to be positive if opposite than the boat speed ($\dot{x}$), is considered in the computation of aerodynamic forces, which are split into drag (F_{ax}) and lift (F_{az}) components:

$$F_{ax} = -0.5\rho(\dot{x} + \dot{x}_w)^2 C_{Da} S_a \qquad (8)$$

$$F_{az} = -0.5\rho(\dot{x} + \dot{x}_w)^2 C_{La} S_a \qquad (9)$$

Due to the particular form of flybridge topsides, several CFD RANS (Reynolds Averaged Navier-Stokes equations) analyses were carried out and new correlations were proposed in order to carefully predict aerodynamic effects on the boat. In detail, in case of heading relative flow (between wind and boat), drag and lift coefficients can be estimated as follow:

$$C_{Da} = 0.5816 - 0.3622\theta \qquad (10)$$

$$C_{La} = 0.18 + 0.125 atan(60\theta - 5.88) \qquad (11)$$

while in the case of following relative flow, the following formulations are proposed:

$$C_{Da} = 1.0336 - 0.8364\theta \qquad (12)$$

$$C_{La} = 0.736 - 2.0784\theta \qquad (13)$$

As it can be observed, the aerodynamic coefficients are function of the sole pitch angle; in fact, it was interestingly observed from CFD analyses that Reynolds number slightly affects the aerodynamic coefficients of the questioned boat.

2.2.2. Powertrain modelling. The "Propeller and Powertrain" subsystem of the digital twin is aimed at predicting the fuel consumption in front of a thrust request (found by means of the balance of forces on the horizontal axis) from the "Boat Dynamics" subsystems. This assembly is required to operate the digital twin in constant (average) speed mode; in fact, since powertrains are commonly controlled in (almost) constant propeller rotating speed, a continuous adjustment of torque is needed (still respecting the engine transients) to cover the thrust request fluctuations due to waves. Since the request to engine depends on the propeller behaviour, even the latter is modelled in this assembly.

The data flow of the "Propeller and Powertrain" subsystem is shown in figure 3.

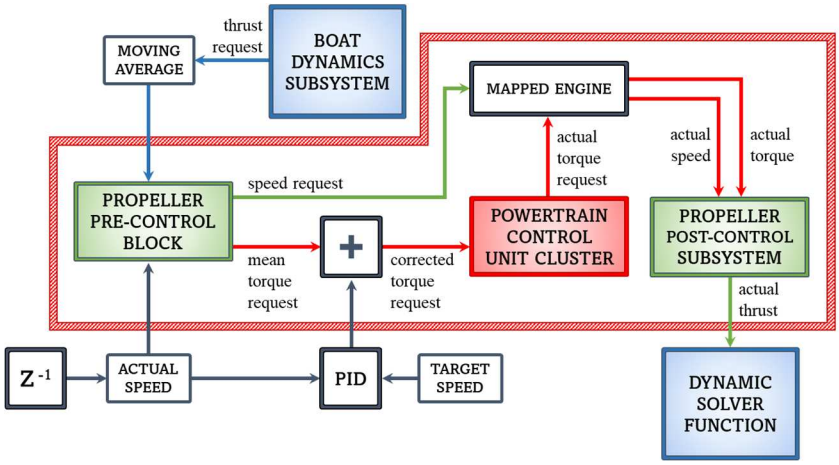

Figure 3. Data flow scheme of the "Propeller & Powertrain" subsystem.

The "Propeller pre-control" assembly receives the (average) thrust request coming from the "Boat Dynamics" subsystem. Here, the constitutive equations of the propeller are implemented, including the experimental characteristic curves, as a function of the advance coefficient, of the 3-620x885 propeller (open-water thrust coefficient, torque coefficient, and efficiency), representing the performance of the propeller in undisturbed water, as well as the thrust deduction factor, wake factor, and relative rotative efficiency, depicting the interaction between hull and propeller, and, finally, the propeller gear-ratio.

To control the propeller in constant speed mode, the estimation of the propeller speed from the thrust request is required. An estimation of the advance coefficient is thus carried out assuming a linear trend of the open-water thrust coefficient in the operating point vicinity. Through the wake factor and gear ratio the propeller and engine speeds can be found. In the same way, the propeller torque can be found through the characteristic curve of the open-water torque coefficient and then the engine torque can be obtained using the gear ratio and the relative rotative efficiency.

The speed and torque requests enter the "Mapped Engine" assembly, in which the steady-state operating maps and the inertial behaviour of the 6LY440J engine are stored. The maps include the torque curve, the BSFC map as a function of load and speed, as well as CO, HC, and CO_2 maps, and were obtained by means of a 1-D imposed-combustion GT-Suite engine model. The experimental heat release curves were implemented by means of the Wiebe function. It should be noted that before entering the "Mapped Engine" block, the torque request is corrected by means of a PID controller targeting the desired speed and then by the "Powertrain Control Cluster" smoothing rapid transients.

The actual engine speed is finally converted into the actual propeller thrust in the "Propeller Post-Control" assembly by evaluating the advance coefficient and then open-water thrust coefficient curve. The thrust signal is finally sent to the "Dynamic Solver" function to solve the equations of motion.

Such propulsion system modelling, thanks to the block structure, can be easily upgraded to also represent hybrid powertrains and innovative components, e.g., electrically assisted turbocharges [24].

2.2.3. Comfort and safety modelling. In [18], a methodology for assessing the safety and comfort of passengers is shown. Thus, only main features are below exposed. It is worth reminding that a proper regulation for assessing comfort and safety in leisure planing boats is nowadays still missing.

Concerning comfort, time-integral indicators should be used, since passengers may prove the same discomfort if subjected to intensive accelerations for small periods and vice versa. In detail, the Root Mean Square (RMS) vertical acceleration at the seat (a_{RMS}) can be investigated in case of crest factors (i.e., ratio between the wk-filtered peak acceleration and the wk-filtered RMS acceleration) lower than 9, as suggested from the ISO 2631-1:1997:

$$a_{RMS} = \sqrt{\frac{1}{T_{path}} \int_0^{T_{path}} a_w^2(t)\, dt} \qquad (14)$$

where a_w is the wk-filtered vertical acceleration at the seat and T_{path} the exposure time. At the same time, the Vibration Dose Value (VDV) at the seat can be investigated for crest factors higher than 9:

$$VDV = \sqrt[4]{\int_0^{T_{path}} a_w^4(t)\,dt} \tag{15}$$

Sickness values for planing boats are not explicitly regulated. The European Directive 2002/44/EC (whole body vibration) provides a_{RMS} and VDV daily sickness limits of 1.15 m/s^2 and 21 m/s$^{1.75}$, which can be used even for planing boats (despite these values are claimed to be highly conservative). Since the daily limit refers to an eight-hours exposure, the limits to be applied in the weather routing model can be obtained through the procedure proposed in the ISO 2631 regulation:

$$a_{RMS} = a_{RMS\_8h}\left(\frac{T_{8h}}{T_{path}}\right)^{\frac{1}{2}} \tag{16}$$

$$VDV = VDV_{8h}\left(\frac{T_{8h}}{T_{path}}\right)^{\frac{1}{4}} \tag{17}$$

In terms of passenger safety instead, the peak vertical acceleration can be considered since high values may lead to spinal injury. In a preliminary and precautionary approach, e.g., a limit value of 2.25g could be accounted [18].

Depending on the crest factor, a_{RMS} and VDV can be adopted in navigation systems as the objective function so as to maximize comfort, or as integral constraints during fuel-based optimizations. The unfiltered peak vertical acceleration at the seats can instead be used as an instantaneous constraint, so as to exclude unhealthy routes from the graph of the optimization algorithm.

2.3. Weather routing system

In this section, the methodology for the acquisition of open-source weather data and the conversion into digital twin inputs is presented; then, the criteria for the direct graph design and the application of the Dijkstra's algorithm are shown. Since these two activities are carried out by two different codes, they will be presented separately. It is worth reminding that the activity goal concerns the development of a smart and flexible weather routing navigation system, accounting for both fuel consumption (thus CO_2 emission) and comfort, depending on the destination of use. It should also be reminded that the use of MATLAB® allows the implementation of the weather routing system on onboard computers.

2.3.1. Weather data acquisition. In order to develop an open-source navigation system, the weather maps of the LaMMA Meteo website ("Mare e Vento" webpage) were chosen, typically considered as a reliable set of data for the Tuscan Archipelago. In detail, wave height, wave period, and wind intensity were accounted; sea currents have been instead neglected, assuming that they slightly affect the dynamics of planing boats. An example of the investigated weather maps is presented in figure 4.

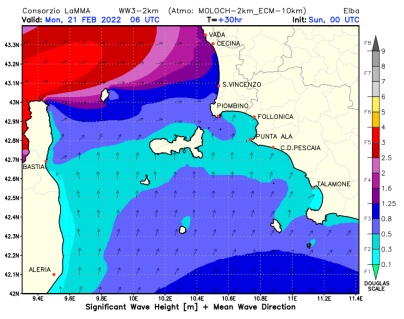

Figure 4 (a). Example of wave height map from LaMMA.

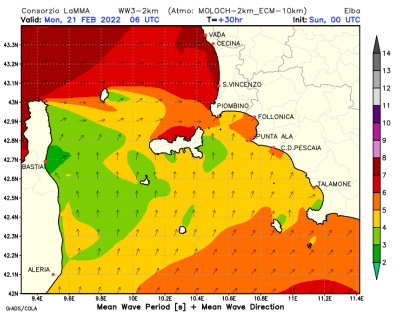

Figure 4 (b). Example of wave period map from LaMMA.

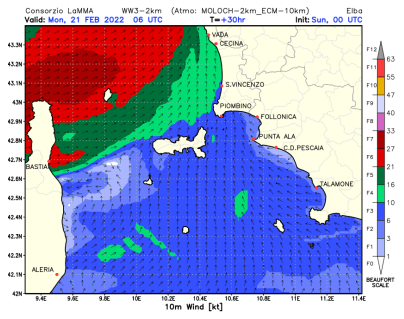

Figure 4 (c). Example of wind map from LaMMA.

In order to provide to the "Weather routing master code" a discrete set of input data, it was firstly required to convert the weather data from a quasi-continuous domain (pixels) to a discrete table. This procedure is carried out by the "Data acquisition slave code". Intensity and direction of the weather variables are presented in a different manner inside the maps; in fact, the former is represented by color characteristics as indicated in the colorbar, while the latter is shown by means of colored arrows. Thus, the data acquisition process has been split in two different procedures (figure 5).

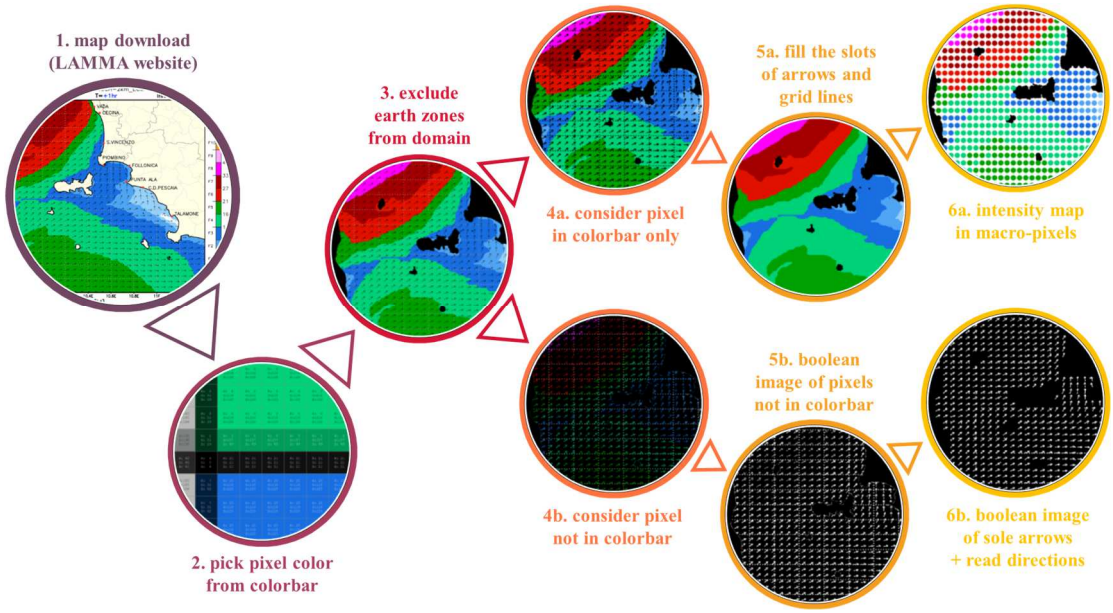

Figure 5. Procedure for the conversion of an example of wind map from the LaMMA Meteo website into the matrixes of intensities and directions.

Considering for example a wind map of the LaMMA website (figure 5), after the download from the webpage and the upload in the workspace, the slave code translates the map in three matrixes, which dimensions correspond to the number of pixels of the map, each one presenting the R, G, and B values of each pixel. The slave code then looks at the colorbar and picks its RGB properties, making them comparable to those on the weather map (figure 5, step 2).

In order to exclude the land zones (specific light-yellow colour in the map) from the navigation zone, the code applies a filter consisting in a sub-code which finds the RGB values of the earth zones on the three R/G/B matrixes and replaces them with null values, i.e., black colour (figure 5, step 3).

Then, the code excludes the arrows from the original map (arrows are made of different colours than the colorbar) by replacing in the three R/G/B matrixes the values not belonging to the colorbar with a null value (figure 5, step 4a). The three R/G/B matrixes are then converted in a single intensity matrix by comparing the colour properties to the colorbar. Null cells, corresponding to arrows only, are filled by averaging the surrounding intensity values (figure 5, step 5a).

The dimensions of the intensity matrix (one cell per each pixel) are then reduced by grouping cells in macro-pixels of 19x15 pixels, to include an entire arrow per each cell. The mode of the intensity of the 285 pixels included in the macro-cell are then used to assign an intensity value (figure 5, step 6a).

Concerning directions, starting from the filtered map, i.e., without earth zones (figure 5, step 3), the slave code firstly assigns a null value to the pixels corresponding to the colormap, thus including only arrows and dotted lines of coordinates (figure 5, step 4b). Then, a Boolean filter is applied, converting the image in a matrix of ones and zeros, i.e., b/w scale (figure 5, step 5b). Dotted lines of coordinates are finally excluded by counting a minimum number of adjacent cells with unity values (figure 5, step 6b). The "regionprops" command allows us to read the direction of arrows (zero direction toward east and counting counterclockwise) and assign the direction value to each non-null cell. Then, the same

operation of dimension reduction of the matrix is carried out, so as to assign a single direction value per each macro-cell.

It is worth pointing out that the number of arrows in the wave hight and wavelength maps of the LaMMA Meteo website are less than those in the wind map. Thus, the original direction matrix of these two weather variables is characterized by cells of 38x30 each. Each cell is thus split in four cells in which the same direction value is used to obtain the same dimensions for all the weather matrixes.

Once that the acquisition process has been repeated for all the weather variables, resulting in three intensity matrixes and two direction matrixes (wave height and wave period have the same directions), a final weather data matrix is written by the slave code. The matrix is composed of seven different columns, representing respectively the coordinates of each macro-pixel, wind intensity and direction, wave height and period, and wave direction. This table is then uploaded by the "Weather routing master code" to assign the weather conditions to the nodes of the direct graph.

2.3.2. Direct graph and Dijkstra's algorithm. Once the weather data matrix has been completed, the "Weather routing master code" draws the direct graph. A diamond form was chosen so as to always consider the minimum length route (main diagonal). The extremities of the main diagonal are put on the selected departure and arrival points; then, several intermediate sections (normal to the diagonal) are considered depending on the desired node distribution. On each section, a certain number of nodes is placed based on the selected growth rate. The width of the diamond is imposed by selecting the ratio between the major and minor diagonals. The connections (single routes) among nodes are drawn by imposing a forward direction only to the boat and assuming that a single node cannot present more than three incoming or leaving connections. This assumption is essentially required to limit the computational cost. In fact, as it will be discussed in detail in Section 3.2, a higher number of connections would lead to trajectories tending to be normal to the major diagonal, which are reasonably unnecessary in case of small/medium leisure planing boats (moderate weather conditions). Finally, the connections ending, starting, or crossing land are discarded. An example of direct graph representing a typical trip from Punta Ala (Pb, Italy) to Bastia (Corse, France) is presented in figure 6, in which seven intermediate sections and a growth rate of two nodes per section were selected, leading to a total of 41 nodes and 68 connections.

Figure 6 (a). Earth filter used to evaluate the sea areas.

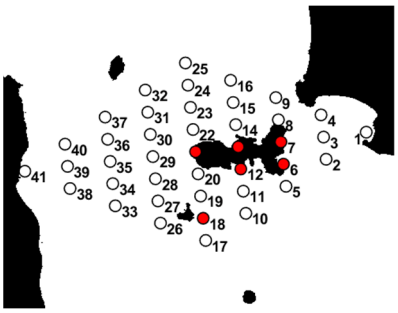

Figure 6 (b). Graph nodes on the map.

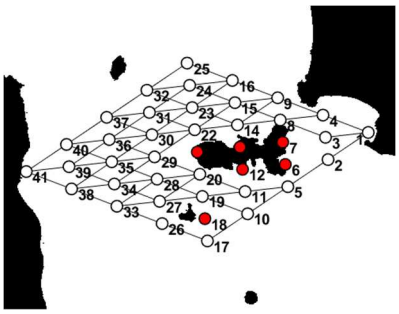

Figure 6 (c). Connections of the direct graph.

Each connection represents a sub-route to be sent in input to the digital twin; thus, to each sub-route, a value of intensity and direction must be assigned per each weather variable. In order to do so, per each node, the values (intensity and direction data) of the closest macro-pixel are assigned, and the average value among the two nodes of the connection is considered.

Once characterized the sub-routes, the master code runs a simulation of the digital twin per each connection. Thus, the fuel consumption, filtered and unfiltered peak vertical acceleration (at the driver seat), and crest factor, are extrapolated and stored in the matrix of results.

The sub-routes in which the safety constraint (i.e., unfiltered vertical acceleration) is exceeded are preventively discarded and signed with a red dashed line on the graph (as it will be seen in figure 10d,

13a and 15a). Finally, the Dijkstra's algorithm searches the optimal path by minimizing the objective function (which can be fuel-based or comfort-based, but also time-based or distance-based, or even a mix among them) among those paths respecting the integral constraints concerning the Wk-filtered vertical RMS acceleration and the VDV.

It is wort noting that standard mesh-based optimization algorithms (like Dijkstra's) do not allow to directly manage state variables (e.g., the boat weight, which decreases moving section-by-section due to the fuel consumption). In fact, it is not possible, in the graph design phase, to assign a priori a state variable to a node which receives in input more than one connection. Thus, in the present activity the weight variation was neglected due to the insignificance of the mass of fuel burned with respect to the total boat weight. This characteristic thus complicates the adoption of the proposed WR methodology in case of hybrid powertrains, in which at least the state-of-charge of the battery must be accounted (even in the simplest control strategy, i.e., the SOC-based control rule, in which the electric power is function of the state-of-charge of the battery). Thus, when dealing with such systems, additional rules for the design of the graph must be added; otherwise, other cell-free optimization methodologies, like dynamic programming, are suggested.

3. Results and discussion

In the present section, several applications of the developed weather routing code are proposed to highlight the potential benefits. The investigated path concerns a leisure trip from Punta Ala to Bastia. The diesel-powered test case boat is considered. Different weather conditions have been investigated.

3.1. Benefits of the weather routing system

This example aims at generally highlighting how the weather routing code could bring to significant benefits in terms of fuel consumption and comfort by selecting a path which differs from the shortest.

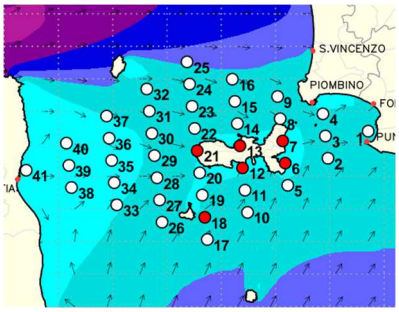

Figure 7 (a). Wave height map with graph nodes, case 1.

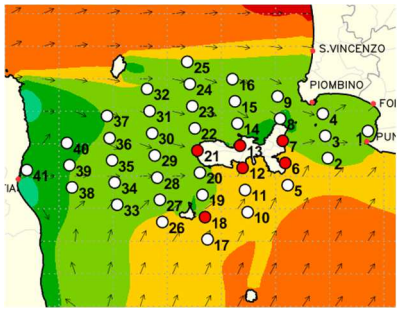

Figure 7 (b). Wave period map with graph nodes, case 1.

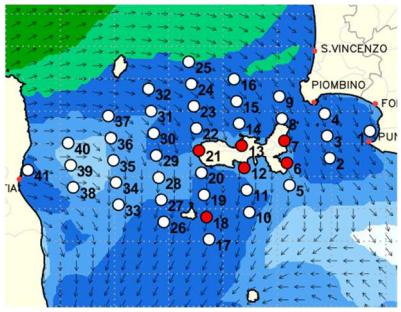

Figure 7 (c). Wind intensity map with graph nodes, case 1.

The considered weather conditions are presented in figure 7. Due to the relatively low-intense wave conditions, a Froude number of 1.2 (i.e., 21.38 kn) was imposed along the entire path. The fuel-based (i.e., minimum fuel consumption) objective function was selected.

Despite the weather maps seem to show a similar behaviour above and below the Island of Elba, the Dijkstra's algorithm found the optimal path to pass below the island (green points in figure 8a), despite the 3.08% longer path than the shortest (pink squares in figure 8a), as it can be seen in figure 8d. In fact, figure 8e presents that at the selected speed, the chosen path leads to a 2.22% lower fuel consumption (figure 8b), despite the longer distance. This behavior is the result of the lower amount of fuel burned in six of eight sub-routes (except the 2nd and the 7th), as it can be observed in figure 8c.

Concerning comfort, the Wk-filtered RMS vertical acceleration was found to be the most suited parameter due to low crest factor (below 9 in the two paths of figure 8a). Only the fuel-optimal path was found to respect the imposed comfort limit (figure 8e); contrarily, the shortest path was found to provide possible sickness for inexperienced passengers due to the short-period oblique waves of the sub-routes 3,4, and 5.

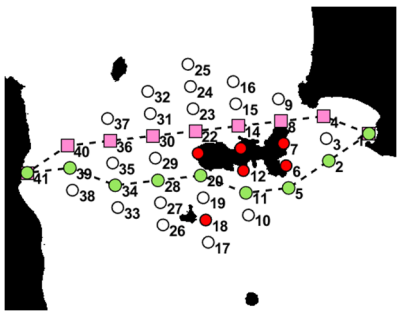

Figure 8 (a). Fuel-optimal and shortest paths on the direct graph.

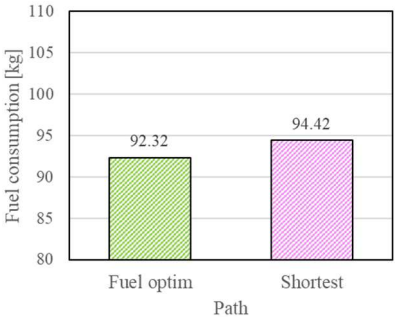

Figure 8 (b). Overall fuel consumption (fuel-optimal and shortest paths).

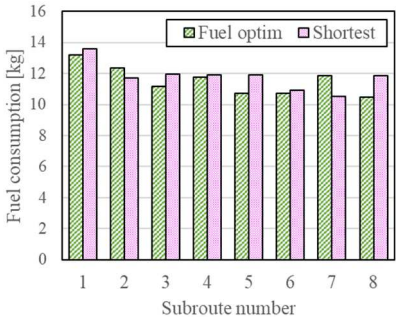

Figure 8 (c). Fuel usage on each route (fuel-optimal and shortest paths).

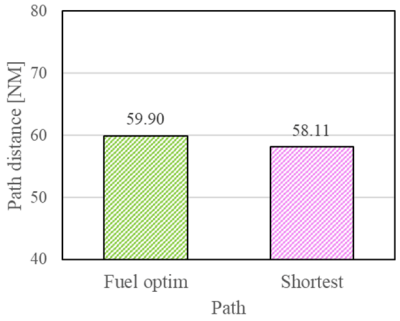

Figure 8 (d). Total travelled distance (fuel-optimal and shortest paths).

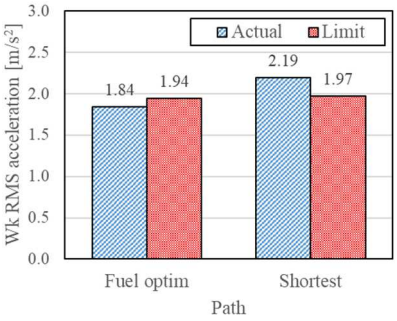

Figure 8 (e). Total filtered RMS acceleration (fuel-optimal and shortest paths).

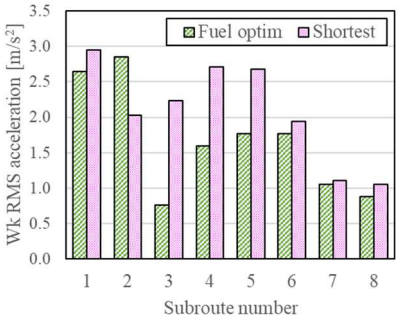

Figure 8 (f). Filtered RMS acceleration on each sub-route (fuel-optimal and shortest).

3.2. Sensitivity to graph definition and guidelines to graph design

The solution of mesh-based optimization algorithms depends on graph shape (i.e., minor-to-major diagonal ratio) and number of nodes (growth rate and number of intermediate sections). Thus, it could be interesting to look, e.g., at the solution provided by the WR code by varying the horizontal graph discretization (number of sections).

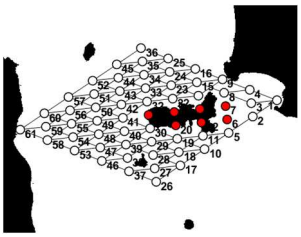

Figure 9 (a). 61-node direct graph.

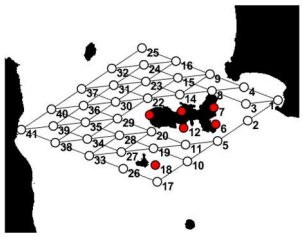

Figure 9 (b). 41-node direct graph.

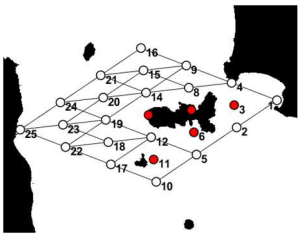

Figure 9 (c). 25-node direct graph.

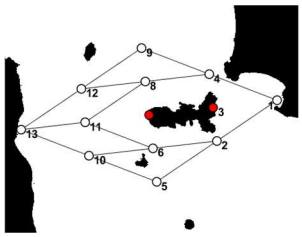

Figure 9 (d). 13-node direct graph.

Four different graphs of diamond shape have been investigated (figure 9), composed of 61 (9), 41 (7), 25 (5), and 13 (3) nodes (intermediate sections) respectively. Boundary conditions, i.e., weather maps and forward speed, are the same of the previous case, as well as the objective function (fuel-based).

By observing the optimal paths (figure 10) it can be noted that the distance of the travel slightly changes, despite the same position of the nodes at the extremities of the minor diagonal (figure 11a). In particular, the 25-node graph led to the longest distance (1.98% longer than the 41-node graph), suggesting the use of a higher number of nodes.

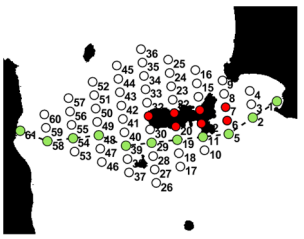

Figure 10 (a). Minim. fuel path (61 nodes).

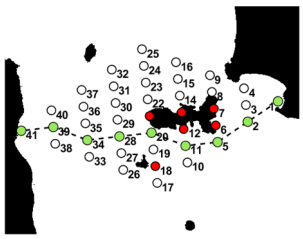

Figure 10 (b). Minim. fuel path (41 nodes).

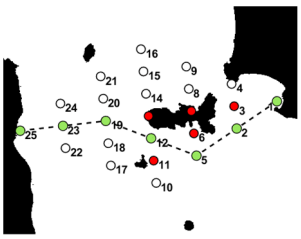

Figure 10 (c). Minim. fuel path (25 nodes).

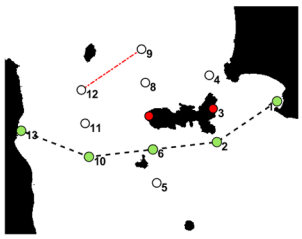

Figure 10 (d). Minim. fuel path (13 nodes).

Concerning fuel consumption, again, the two less-defined graphs (13 nodes and 25 nodes) falsely led to a lower fuel usage than the others (figure 11b). Interestingly, the 25-node graph brought to the lowest fuel usage despite the longest distance, indicating a different acquisition of weather data (due to the different position of nodes).

Concerning instead comfort (figure 11c), only the 13-node graph led to a wrong estimation, since the unconstrainted fuel-optimal solution actually provided a non-acceptable Wk-filtered RMS vertical acceleration. On the contrary, almost the same comfort value was found by means of the other graphs.

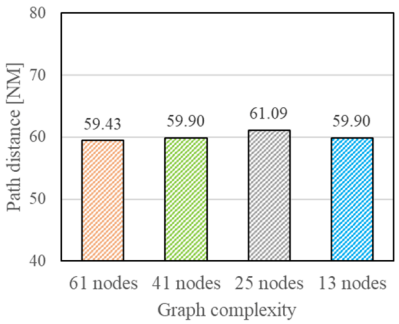

Figure 11 (a). Travel distance varying graph complexity.

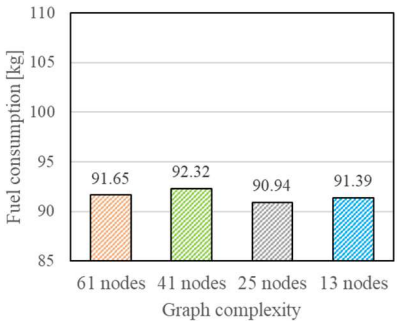

Figure 11 (b). Total fuel usage varying graph complexity.

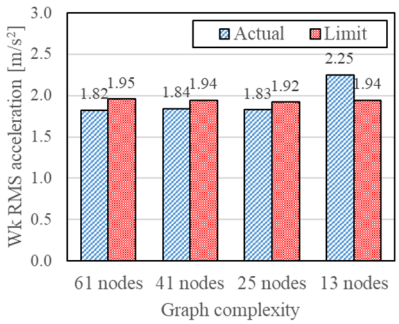

Figure 11 (c). Filtered RMS acceleration varying graph.

Results thus discourage the use of low-definition graphs (25 and 13 nodes), but do not explicitly indicate which of the two high-definition graphs should be used. Anyway, in the investigated weather conditions, the adoption of the 61-node graph led to a 0.73% lower fuel usage, 0.96% lower vertical acceleration and a 0.78% lower travelled distance, in front of a 38% higher calculation time. Thus, since the difference of the investigated variables among the two graphs is always lower than 1%, the 41-node graph was chosen as the baseline configuration in the present activity, especially considering that the destination of use of the proposed code requires low computational times (off-line weather routing is thought to provide results during departure phase from port).

It is worth noting that the choice of adopting no more than three connections per node also follows this strategy. In fact, the use of five connections in the 41-node graph would lead to 104 simulated sub-routes (instead of 68), resulting in a 53% higher computational cost. Vertically tilted connections would be useful when dealing with wavy or stormy conditions, in which a relevant change of the forward direction could be required; however, when dealing with leisure planing boats, which are not suited to stormy navigation, the assumption of reducing the number of connections can be considered a good choice for improving the computation cost, allowing the adoption of a higher number of nodes.

It could be also useful to add some notes on the selection of the growth rate, since it defines the number of nodes of the sections (and really affects the computational cost). The choice of the growth rate, as well as the number of sections, should be related to the distribution of the iso-lines of the weather variables on the map. In the present activity, it was chosen to add two node per section since, in this geographic area, iso-lines tend to assume a horizontal shape (i.e., vertically distributed), thus

requiring the nodes to be vertically close among them. On the contrary, in the case of horizontally distributed iso-lines, it would be preferable to limit the growth rate while increasing the number of intermediate sections. An interactive code for the design of the graph depending on weather variables distribution can thus be an interesting feature for such systems and is postponed to future studies.

3.3. Sensitivity to the objective function (time vs. comfort)

The present example aims at investigating the effects of adopting a different objective function. In particular, it could be interesting to evaluate how a comfort-based solution would differ from the fuel-based optimum. In fact, it is worth reminding that the Dijkstra's algorithm (in the classic set-up) is able to find the global optimum in mesh-based single-objective optimization problems; thus, only a single objective function can be used.

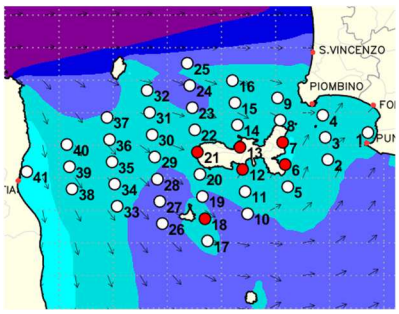

Figure 12 (a). Wave height map with graph nodes, case 2.

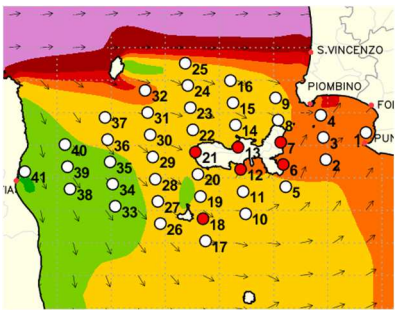

Figure 12 (b). Wave period map with graph nodes, case 2.

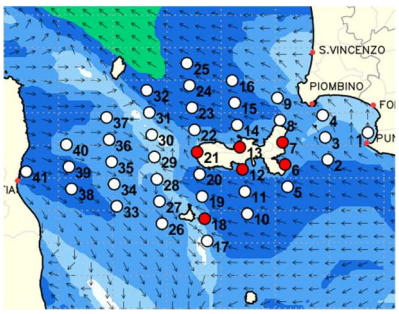

Figure 12 (c). Wind intensity map with graph nodes, case 2.

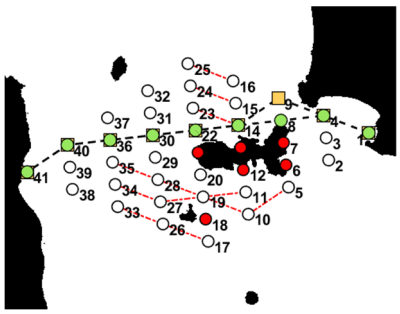

Figure 13 (a). Fuel-based and comfort-based optimal paths and unsafe sub-routes.

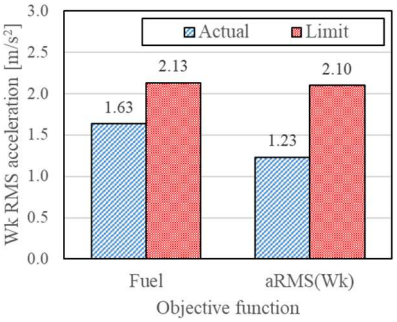

Figure 13 (b). Total filtered RMS acceleration (fuel-based and comfort-based paths).

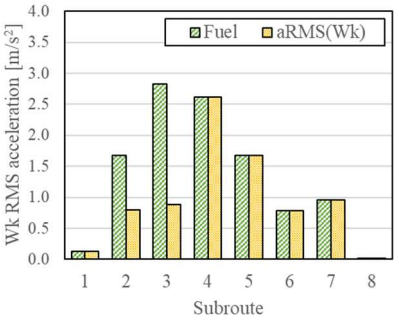

Figure 13 (c). Filtered RMS acceleration on each route (fuel- and comfort-based).

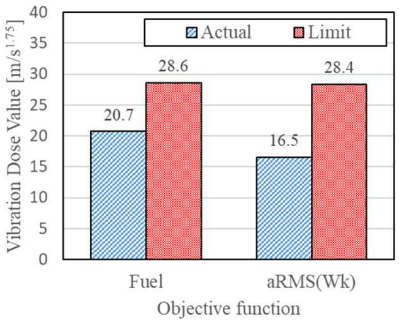

Figure 13 (d). Total Vibration Dose Value (fuel-based and comfort-based paths).

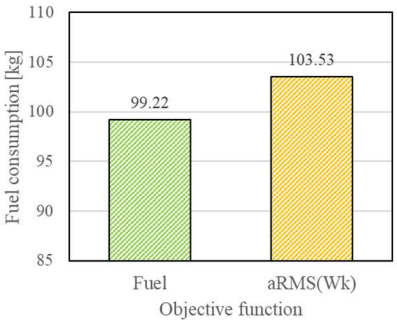

Figure 13 (e). Overall fuel consumption (fuel-based and comfort-based paths).

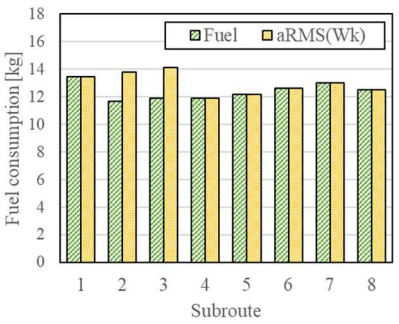

Figure 13 (f). Fuel usage on each route (fuel- and comfort-based).

The weather maps of figure 12 were considered. Due to the relatively calm conditions investigated, a Froude number of 1.4, corresponding to 24.94 kn, was imposed.

In the present case, the different objective functions led to an optimal path which differs in the 2nd and 3rd sub-routes only (figure 13a). Despite that, the comfort-based function (minimum Wk-filtered RMS vertical acceleration) led to a very small Wk-filtered RMS vertical acceleration (24.54% lower than in the fuel-based optimization), as it can be observed in figure 13b, and to a 20.29% lower vibration dose value (figure 13d), indicating the high influence of the two sub-routes (figure 13c); on the contrary, the fuel-based optimization provided a 4.16% lower fuel consumption (figure 13e) mainly as a consequence of the shorter distance (figure 13f).

The preferred objective function thus strictly depends on the destination of use. If unexperienced people or children are involved, it may be worth using a comfort-based objective function, so as to minimize the probability to provide sickness; otherwise, the fuel-based strategy will always ensure the minimum CO_2 emission while still ensuring an acceptable comfort level.

It is anyway worth pointing out that even if the Dijkstra's algorithm does not explicitly allow the use of multiple objective functions, a hybrid objective function, involving more than a single variable, can also be defined. In fact, it would be enough to make dimensionless the investigated variables (e.g., fuel consumption, vertical acceleration, distance, time) by means of reference values and then define a weighted average in which weights are chosen depending on the importance of each variable.

3.4. Influence of weather conditions

The last analysis aims at evaluating the impact on fuel usage of each weather variable. In order to do so, four different optimization problems were run, concerning respectively calm sea and no wind, calm sea with wind, wavy sea and no wind, and, finally, wavy sea with wind. Weather conditions of figure 14 were investigated. An imposed speed of 24.94 kn (Fn=1.4) was considered and the fuel-based objective function was used. The fuel-optimal path chosen by the Dijkstra's algorithm by accounting for the whole set of weather variables (figure 15a) was considered in all the investigated cases.

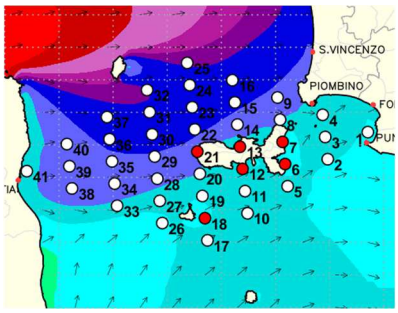

Figure 14 (a). Wave height map with graph nodes, case 3

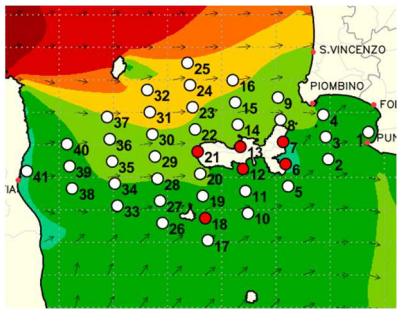

Figure 14 (b). Wave period map with graph nodes, case 3

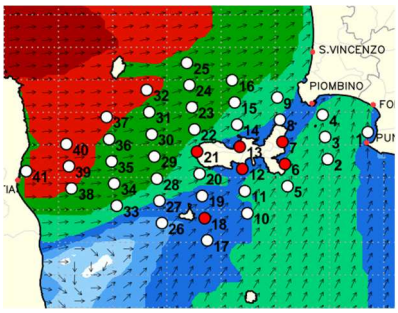

Figure 14 (c). Wind map with graph nodes, case 3

As it can be observed from figure 15b, the sole wind led to a 6.29% higher fuel usage than calm weather operation, despite the moderate wind flow, clearly indicating that aerodynamic aspects cannot be neglected. Comparing again to the calm weather case, the sole waves increased fuel consumption of 19.55%; thus, the added resistance in waves must be carefully accounted in the dynamic model in order not to select wrong paths. Finally, accounting for both wind and waves led even to a 26.43% higher fuel consumption than the calm case. This sensitive difference is especially due to the wave forces in the last two sub-routes (figure 15c), where the boat encounters small period (2 ÷3 seconds) and moderate height (0.5÷0.8 meters) heading waves.

This analysis thus showed the role of carefully modelling the boat dynamics in wind and waves, since an approximative modelling may lead to relevant errors especially in the prediction of the fuel consumption.

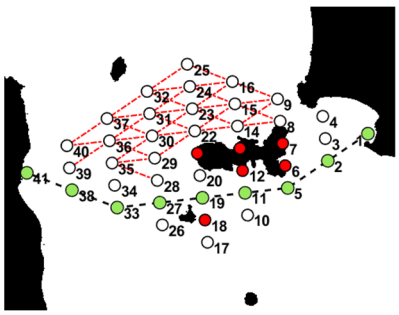

Figure 15 (a). Fuel-optimal path (all weather variables case) and unsafe sub-routes.

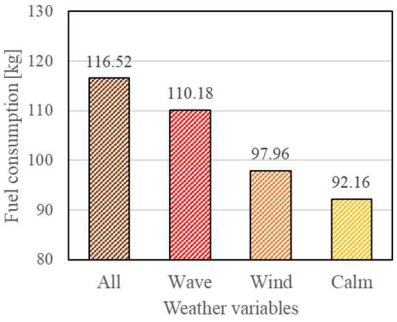

Figure 15 (b). Total fuel usage varying the considered weather variables.

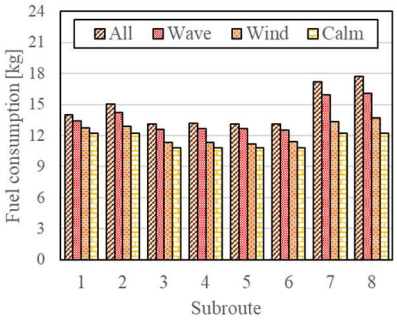

Figure 15 (c). Fuel usage on each route varying the considered weather variables.

4. Conclusions and final remarks

In addition to safety and comfort, the reduction of fuel usage is becoming crucial for leisure crafts in front of the increasingly higher fuel price and stringent regulations. New electronic components paved the way to more effective navigation systems even for leisure planing crafts, in which weather routing (WR) can be adopted to reduce fuel usage and to ensure safety and comfort. Thus, the present study showed a prototype of smart navigation system, developed in the MATLAB® language, based on an improved 2D+t model of a 10-meter planing boat and a WR code based on the Dijkstra's algorithm. The WR numerical tool was designed to optimize fuel consumption while accounting for safety and comfort. After presenting a methodology to acquire and encode the graphical weather data from the LaMMA Meteo website, few applicative examples in the Tuscan Archipelago were shown to prove the potential of an onboard application. It was observed that even in moderate weather conditions, the optimal path (which differs from the shortest one), can lead to both fuel savings and comfort enhancement (-2.22% fuel usage and -15.98% vertical RMS acceleration in a leisure trip from Punta Ala to Bastia). Moreover, it was seen that a comfort-based objective function can be useful when inexperienced people and/or children are involved. In order to establish guidelines for the development of WR systems, a sensitivity analysis on the graph discretization showed that a low-definition graph may lead to a wrong prediction of fuel consumption and comfort, as well as an unsmooth path. Furthermore, an analysis on the influence of each weather variable highlighted the importance of an accurate dynamic modelling, suggesting that simplified or steady-state models cannot be adopted in case of planing boats. The present paper thus showed the impact that the developed technology may offer for a commercial application, moving towards a greener navigation even in local areas.

Acknowledgments

The Authors would like to acknowledge *Dr. Lorenzo Bosi* and *Dr. Alberto Baroni* for contributing to the conceptualization of the present study and the supervision of the results.

References

[1] Wang H, Mao W and Eriksson L 2017 Benchmark study of five optimization algorithms for weather routing *Proc. ASME 2017 36th Int. Conf. on Ocean, Offshore and Arctic Engineering (Trondheim, NO)* **7B** 1-9 https://doi.org/10.1115/OMAE2017-61022

[2] Lee S-M, Roh M-I, Kim K-S, Jung H and Park J J 2018 Method for a simultaneous determination of the path and the speed for ship route planning problems *Ocean Eng.* **157** 301–12 https://doi.org/10.1016/j.oceaneng.2018.03.068

[3] Walther L, Rizvanolli A, Wendebourg M and Jahn C 2016 Modeling and optimization algorithms in ship weather routing *e-Navi* **4** 31–45 https://doi.org/10.1016/j.enavi.2016.06.004

[4] Hagiwara H and Spaans J A 1987 Practical weather routing of sail-assisted motor vessels *J. Navig.* **40** 1 96–119 https://doi.org/10.1017/S0373463300000333

[5] Rabaud M 2016 Optimal routing in sailing *Proc. Conf. Sport Physics (Palaiseau, FR)* 1-6
[6] Szlapczynska J and Smierzchalski R 2007 Adopted isochrone method improving ship safety in weather routing with evolutionary approach *Int. J. Reliab. Qual. Saf. Eng.* **14** 6 635–45 https://doi.org/10.1142/S0218539307002842
[7] Zoppoli R 1972 Minimum-time routing as an n-stage decision process *J. Appl. Meteorol. Climatol.* **11** 3 429–35 https://www.jstor.org/stable/26175736
[8] Aligne F, Papageorgiou M and Walter E 1998 Incorporating power variations into weather routeing and why it may lead to better results *IFAC Proceedings Volumes* **31** 30 269–74 https://doi.org/10.1016/S1474-6670(17)38451-3
[9] Shao W, Zhou P and Thong S K 2012 Development of a novel forward dynamic programming method for weather routing *J. Mar. Sci. Technol.* **17** 239–51 https://doi.org/10.1007/s00773-011-0152-z
[10] Zaccone R, Ottaviani E, Figari M and Altosole M 2018 Ship voyage optimization for safe and energy-efficient navigation: a dynamic programming approach *Ocean Eng.* **153** 215–24 https://doi.org/10.1016/j.oceaneng.2018.01.100
[11] Kim B and Kim T-W 2017 Weather routing for offshore transportation using genetic algorithm *Appl. Ocean Res.* **63** 262–75 https://doi.org/10.1016/j.apor.2017.01.015
[12] Hinnenthal J and Clauss G 2010 Robust pareto-optimum routing of ships utilising deterministic and ensemble weather forecasts *Ships and Offshore Struct.* **5** 2 105–14 https://doi.org/10.1080/17445300903210988
[13] Takashima K, Mezaoui B and Shoji R 2009 On the fuel saving operation for coastal merchant ships using weather routing *TransNav* **3** 4 401-406
[14] Sen D and Padhy C P 2015 An approach for development of a ship routing algorithm for application in the North Indian Ocean region *Appl. Ocean Res.* **50** 173–91 https://doi.org/10.1016/j.apor.2015.01.019
[15] Mannarini G, Coppini G, Oddo P and Pinardi N 2013 A Prototype of ship routing decision support system for an operational oceanographic service *TransNav* **7** 53-59
[16] Pennino S, Gaglione S, Innac A, Piscopo V and Scamardella A 2020 Development of a new ship adaptive weather routing model based on seakeeping analysis and optimization *J. Mar. Sci. Eng.* **8** 4 270 1-16 https://doi.org/10.3390/jmse8040270
[17] Savitsky D 1964 Hydrodynamic design of planing hulls *Mar. Technol. SNAME N.* **1** 04 71–95 https://doi.org/10.5957/mt1.1964.1.4.71
[18] Ciampolini M, Balduzzi F, Romani L, Bellucci L, Bianchini A and Ferrara G 2022 Development of an improved and versatile 2D+t modelling methodology for planing crafts *Ocean Eng.* **265** 1–23 https://doi.org/10.1016/j.oceaneng.2022.112617
[19] Zarnick E E 1978 A nonlinear mathematical model of motions of a planing boat in regular waves *(Bethesda, US: David W. Taylor Naval Ship Research and Development Centre Report)*
[20] Payne P R 1994 Recent developments in "added-mass" planing theory *Ocean Eng.* **21** 3 257–309 https://doi.org/10.1016/0029-8018(94)90002-7
[21] Wagner H 1931 Landing of seaplanes *(Washington, US: National Technical Information Service Report)*
[22] Payne P R 1995 Contributions to planing theory *Ocean Eng.* **22** 7 699–729 https://doi.org/10.1016/0029-8018(94)00033-4
[23] Faltinsen O M, Minsaas K J, Liapis N and Skjordal S O 1980 Prediction of resistance and propulsion of a ship in a seaway *Proc. 13th Symp. on Naval Hydrodynamics (Tokyo, JP)*
[24] Ciampolini M, Fazzini L, Berzi L, Ferrara G and Pugi L 2020 Simplified approach for developing efficiency maps of high-speed PMSM machines for use in EAT systems starting from single-point data *2020 IEEE Int. Conf. on Environment and Electrical Engineering and 2020 IEEE Industrial and Commercial Power Systems Europe (Madrid, ES)* 1-6 doi: 10.1109/EEEIC/ICPSEurope49358.2020.9160775